

# Control authority over a combustion instability investigated in CFD

Roel AJ Müller<sup>1</sup>, Jakob Hermann<sup>1</sup> and Wolfgang Polifke<sup>2</sup>

## Abstract

Control authority is investigated for active damping of a combustion instability by modulation of the fuel flow. Two combustors, operating as quarter-wave thermo-acoustic oscillators, are modelled in ANSYS CFX. In experiments, active damping was applied successfully on one of these, but was not effective on the other. Active instability control is implemented in the model analogous to experiment. The goal of this research is to explain why the same implementation of active instability control, using the same controller, would be effective on one combustor geometry, but not on the other. Turbulent combustion is modelled by SAS-SST and the burning velocity model. The distribution of the convective time between fuel injector and flame is evaluated and used to estimate the response of the heat release to modulation of the fuel mass flow. The results can be used to predict the feasibility of this kind of active control.

## Keywords

Combustion dynamics, self-excited thermoacoustic instability, active control, control authority, turbulent combustion modelling

Date received: 18 July 2014; accepted: 3 May 2015

## Introduction

This paper describes the simulation of combustion instabilities occurring in two model combustors. Combustion instabilities are a major problem in industrial gas turbines. Strong pressure oscillations can cause severe hardware damage, while even weaker oscillations can cause an increase in pollutants. For a thorough introduction to the issues associated with combustion instabilities, as well as possible solutions, the reader is referred to Culick.<sup>1</sup>

### *State of the art in active damping of combustion instabilities*

A possible remedy for combustion instabilities is the application of Active Instability Control (AIC). Compared to passive damping features, such as Helmholtz resonators, AIC has the advantage of being more flexible in application: one AIC system can attenuate multiple modes of oscillation. Especially for lower frequencies (say <500 Hz), the sensors and actuators needed for AIC are much smaller than passive dampers effective in the same frequency range. As a result, AIC usually needs smaller structural

modifications than passive measures when retrofitting a turbine with instability issues.

Many successful lab-scale demonstrations of AIC have been reported in the literature. For example: Lang et al.<sup>2</sup> use a loudspeaker in the plenum between fuel injection and flame in a premixed propane combustor, Bloxside et al.<sup>3</sup> use a valve at a similar position in a premixed propylene combustor, Heckl<sup>4</sup> uses a loudspeaker placed at the downstream end of a Rijke tube, and Hermann et al.<sup>5</sup> use a piezo actuator in the fuel supply line of a liquid fuel combustor. More recent reviews are given, for instance, by Dowling and Morgans<sup>6</sup> and Culick and Palm.<sup>7</sup>

While most examples of AIC are found on a laboratory scale, Hermann and Orthmann<sup>8</sup> are a notable exception, using a direct drive valve by Moog Inc. in the fuel supply line to apply AIC on a heavy-duty

<sup>1</sup>IfTA Ingenieurbüro für Thermoakustik GmbH, Gröbenzell, Germany

<sup>2</sup>Professur für Thermofluidynamik, Technische Universität München, Garching, Germany

#### Corresponding author:

Roel AJ Müller, IfTA Ingenieurbüro für Thermoakustik GmbH, 82194 Gröbenzell, Germany.  
Email: info@ifta.com



industrial gas turbine. However, further commercial application remains challenging due to the unpredictability of control authority.

### Goal of current research

The current research investigates the application of control authority in the cases of two combustors, showing a low-frequency thermo-acoustic oscillation, often referred to as ‘humming’. Since the current research was started as a part of the EU-funded project LIMOUSINE (FP7-214905; *Limit* cycles of thermo-acoustic oscillations in gas turbine combustors), one of the combustors investigated here is the model combustor of the project, referred to as the ‘Limousine’ for brevity. The other combustor under consideration is one of the prototype combustors, constructed at IfTA during the start-up phase of the project.<sup>9</sup> Since the instability of this combustor is at times louder and generally lower in frequency, it will appropriately be referred to as the ‘Hummer’. Both combustors will be discussed in more detail in the next section.

Experimental application of active control worked well on the Hummer, but not on the Limousine test rig. Figure 1 shows spectra of both combustors with and without active control. Since the same controller was used on both combustors, the difference in control authority has to be caused by the geometrical differences between the combustors. This paper describes the simulation of both combustors in ANSYS CFX in an effort to find the cause of this difference in control authority.

Although there are examples of combustion simulations with active control in literature, such as

Menon<sup>10,11</sup> and Shinjo et al.,<sup>12</sup> the current research gives a comparison between a case of unsuccessful and one with successful control. The goal is to gain better insight into the mechanisms required for successful application of active control on combustion instabilities.

## Set-up

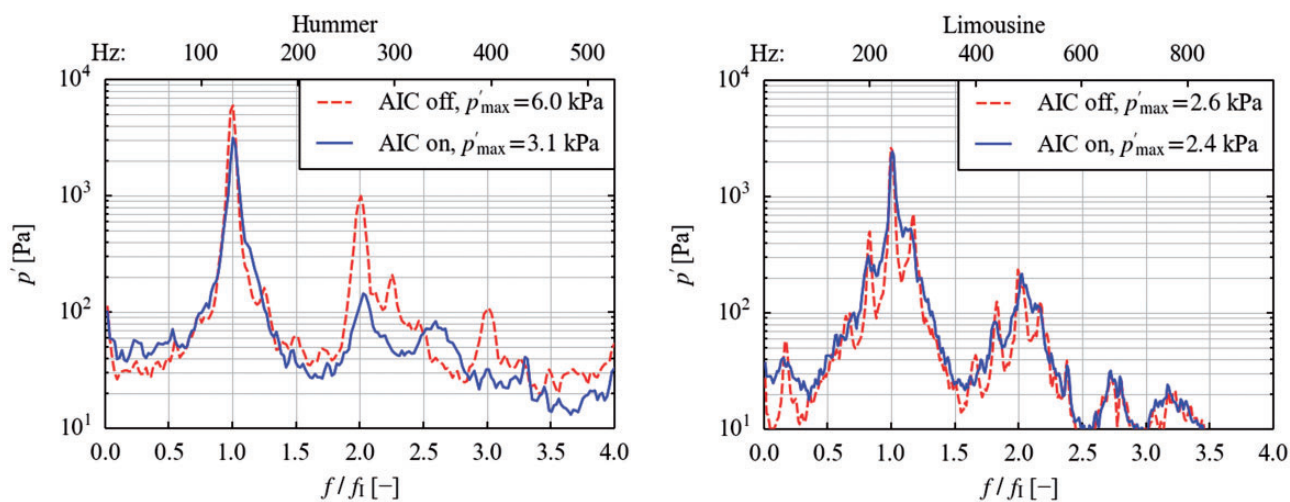
### Combustor geometry and grid

Figure 2 gives an overview of the simplified geometries and dimensions for both combustors, as used in CFX. The burner is situated in a duct of rectangular cross section with closed/open acoustic boundary conditions, approximating a quarter-wave acoustic resonator. The rectangular cross section with relatively large aspect ratio leads to an approximately 2D flow in the  $x, y$  plane. The computational domain takes advantage of this, representing only a thin slab of the combustor, with symmetry boundary conditions applied on both sides.

For the Hummer, the inner span in  $z$  direction is 180 mm, while the computational domain has a thickness of 2.5 mm. For the Limousine rig, the physical and computational span are 150 mm and 2 mm, respectively.

The pressure at  $x = -200$  mm (labelled ‘sensor’ in Figure 2) is sampled and passed to the controller as input. The origin of  $x$  is at the top of the flame holder. Note the fuel injector holes of the Limousine are situated further upstream than those of the Hummer, in an effort to improve mixing of fuel and air.

The (choked) air inlet is modelled as a fixed mass-flow boundary condition. The open outlet is modelled



**Figure 1.** Spectra of pressure oscillation in both combustors with and without active control, running at thermal power  $P_{th} = 40$  kW and equivalence ratio  $\Phi = 0.71$  ( $\lambda = 1.4$ ).

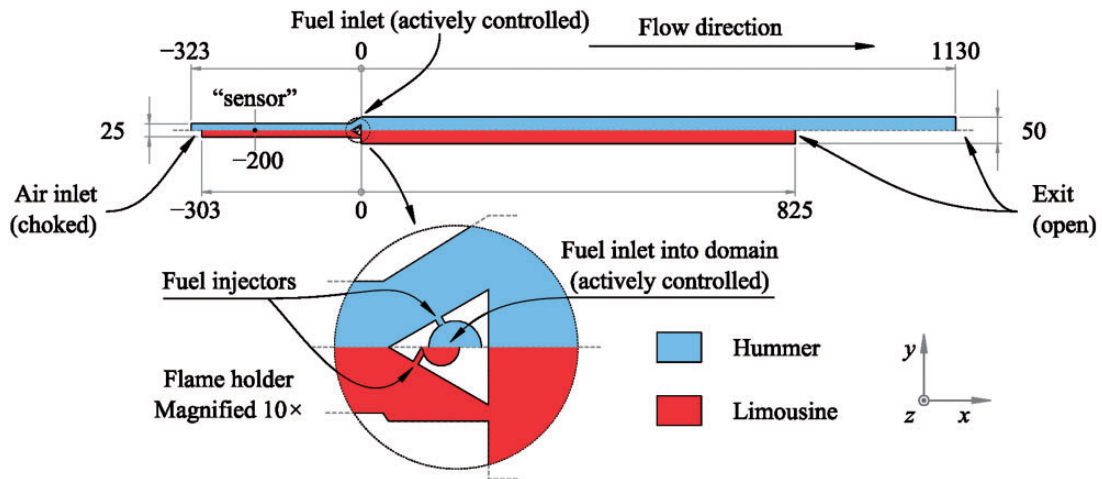


**Figure 2.** Overview of the computational domain for both combustors: Hummer (blue) above and Limousine (hatched in red) below. Dimensions are in mm.

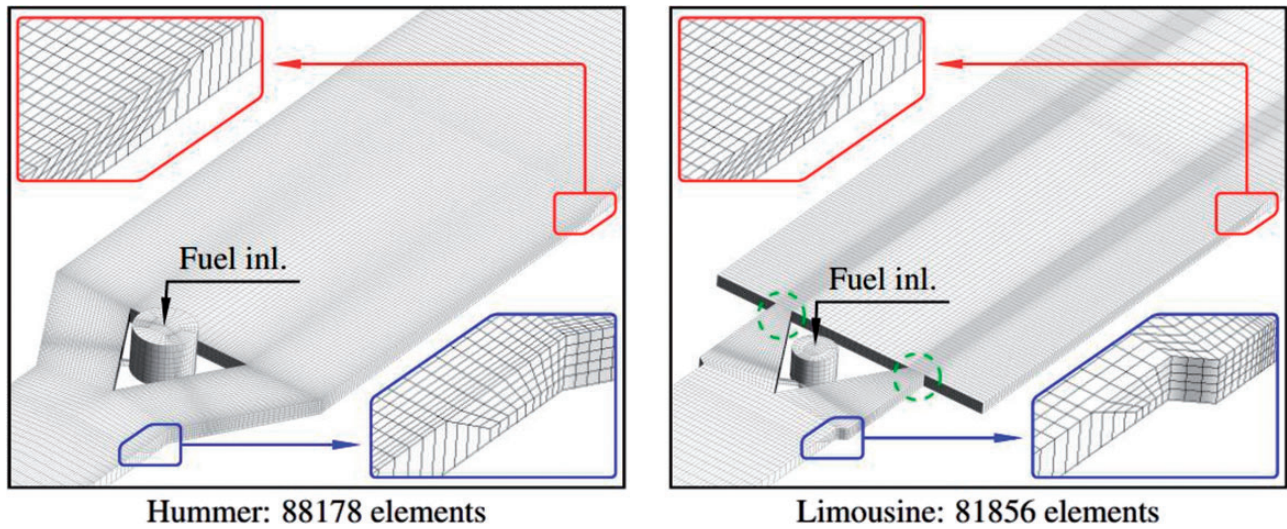


**Figure 3.** Detail of the 3D grid region with transitions to 2D. Hummer on the left. For Limousine on the right, note the narrow slits (circled) on either side of the flame holder.

as an opening (allowing in- and out-flow) at constant pressure. The prismatic flame holder, triangular in cross section, is at about one-quarter of the length ( $x$ ) of the combustor. Fuel gas (methane) is distributed through the flame holder and injected into the airflow through injector holes along the span ( $z$ ) of the flame holder. The computational domain includes half an injection hole on either side of the flame holder. The fuel mass flow can be modulated by the controller. The partially premixed flame is stabilised downstream of the flame holder. There is a small volume between the fuel inlet and the injector holes (see also Figure 2) to represent the compliance of the fuel supply system downstream of the AIC actuator.

Both computational grids are structured meshes of hexahedral elements. The grids are 2D in the plenum and the downstream end of the combustion chamber, where gradients in  $z$  direction are negligible, to save computational cost. The region around the flame holder and extending downstream is three-dimensional, to resolve the intrinsically three-dimensional mixing of the fuel jet into the cross-flow of air. Figure 3 shows this 3D region and the transitions to 2D.

The liner walls are modelled as thermally conductive no-slip walls with a heat transfer coefficient of  $50\text{W}/(\text{m}^2\text{K})$ , based on an estimate of the heat loss by free convection and radiation towards an environmental temperature of 300 K.

### Computational model

The transient simulation in ANSYS CFX v14.5 used eight cores, with  $10^{-5}$  s time steps. The thermal power  $P_{th} = 40$  kW, and the equivalence ratio  $\bar{\Phi} = 0.71$  ( $\lambda = 1.4$ ). Turbulence is modelled with the Scale Adaptive Simulation model (SAS-SST) model.<sup>13</sup> Combustion is simulated by the Burning Velocity Model, using a new model option for improving accuracy for non-premixed flames.<sup>14–17</sup> Other combustion models such as the eddy dissipation model and the Extended Coherent Flame Model were used in preliminary simulations, but gave an oscillating behaviour which agreed less with experiment.

A practical advantage of the Burning Velocity Model is that the volumetric heat release rate is readily available for post processing. In the remainder of this section, this information will be used to estimate optimal controller settings.

### Implementation of active control in CFX

The controller is identical to the one used by Hermann and Orthmann.<sup>8</sup> In simple terms, it behaves like an amplification plus phase shift, which can be set according to preferences. The precise workings of the controller are kept confidential, to protect the commercial interests of IFTA. The same controller is used in both cases, so that the controller can be ruled out as the cause of the difference in control authority.

The controller runs as a command line application which reads a log file with under-sampled (in time) pressure data from the sensor position and writes the output value to another file. In CFX, a user function (written in FORTRAN) updates the pressure log file and reads the output value from the controller. The fuel inlet mass flow is varied according to the controller output.

The goal is to damp the oscillation by reduction of Rayleigh's coefficient.<sup>18</sup> The equivalence ratio is modulated to cause a fluctuating heat release rate ( $\dot{Q}'$ ) in opposite phase with the pressure fluctuation  $p'_{\dot{Q}}$  at the flame. The controller does, however, not know the pressure at the flame directly, since the pressure probe supplying the controller input is situated further upstream, at  $x = -200$  mm; neither can it influence the heat release at the flame instantaneously. In experiment or industrial operation, relatively long time series of input data are available to converge to the optimal phase shift. For numerical simulation, another approach is needed. Here, the phase shift between the pressure at the AIC input sensor and the pressure at the flame can be determined from the mode shape of the oscillating combustor. The time-lag between a fuel mass-flow fluctuation caused by the controller and the corresponding heat release fluctuation is mainly caused by the

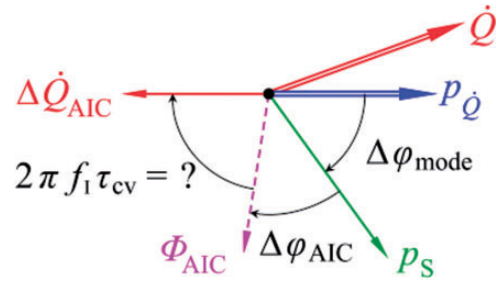


**Figure 4.** Phase plot giving an overview of the various phase lags relevant for active damping of combustion instability by modulation of the fuel flow. Amplitudes are not to scale. The phase of  $p'_{\dot{Q}}$  is defined as zero. A resulting phasor  $\dot{Q}$  to the right implies a positive Rayleigh coefficient.

convective time between the fuel injector and the flame. Figure 4 gives an overview of the relevant processes.

The controller phase shift is defined positive for a phase lag. The value required for a heat release in anti-phase with the pressure fluctuation is found as

$$\arg \frac{p'_{\dot{Q}}}{p'_S} + (\tau_{ac} + \tau_{cv})2\pi f_I + \Delta\phi_{AIC} = (2n + 1)\pi \quad (1)$$

where  $f_I$  is the frequency of the dominant oscillation.  $\arg(p'_{\dot{Q}}/p'_S)$  represents the phase difference between the pressure fluctuation  $p'$  at the sensor (S) and at the flame ( $\dot{Q}$ ). Together with the phase shift caused by acoustic (ac) and convective (cv) delay, and the phase shift set for the controller, this should add up to  $n$ -and-a-half oscillation cycles. Regarding the fuel system as a Helmholtz resonator, its resonance frequency is much higher than that of the oscillation at hand. Therefore, the fuel system can be regarded as a pure acoustic compliance, and the acoustic time delay between fuel inlet and fuel injector can be neglected ( $\tau_{ac} \approx 0$ ). Since  $\tau \approx \tau_{cv}$ , the subscript 'cv' will be dropped in the following. The compliance remains significant, so the fuel system should still be included in the computational domain. In reality,  $\tau$  is not single-valued, but forms a spatial distribution over the flame. Since the flame is unstable, this distribution varies in time as well. This has serious consequences for the control authority, which will be discussed in 'Controller settings and analysis of the convective time delay' section.

### Definition of the convective time

Following the procedure proposed by Krebs and Lohrmann,<sup>19</sup> the convective time of fuel 'parcels' from the fuel inlet  $\tau(\vec{x}, t)$  towards the flame is computed as an additional field variable. In this approach, two auxiliary field variables, each representing passively convected scalars, are defined:  $C_i(\vec{x}, t)$  and  $C_1(\vec{x}, t)$ .

At the air inlet, the boundary conditions are set to  $C_1 = C_t = 0$ . At the fuel inlet, the boundary conditions are  $C_1 = 1$  and  $C_t = t$  (the simulation time at which the fuel entered the domain). The expression  $C_t/C_1$  remains constant when the fuel expands, mixes with air, or gets consumed in the flame. Its value represents the time at which the fuel (or corresponding combustion products) enters the domain. The variable  $\tau(\vec{x}, t) = t - C_t/C_1$  represents thus the convective time from the fuel inlet, viz. the boundary of the domain, to the location  $\vec{x}$ . This method will be less reliable in situations with recirculation, where  $\tau$  will be a mixture of the convective time for the direct route, and the route with circulation, but this is thought to be a lesser influence in the current situation.

In the present configuration, there is an additional complication. The quantity of interest is not the time since the fuel entered the computational domain into the fuel supply, but instead the time which has passed since fuel was injected out of the fuel supply system into the air flow. Recall the detail of Figure 2, where the injectors and inlet into the domain are labelled. To get the desired result, the diffusion coefficient of both  $C_t$  and  $C_1$  was set to  $10^4 \text{ m}^2/\text{s}$  inside the fuel supply system, and zero elsewhere. This way,  $C_t = t$  and  $C_1 = 1$  still hold at the exit of fuel injector tubes, and  $\tau$  represents the convective time from there on.

As done by Polifke et al.,<sup>20</sup> a distribution of convective time lags  $\tau$  will be interpreted in the form of a histogram of the heat release rate  $\Delta\dot{Q}_i$  plotted against  $\tau_i$ . While Polifke et al. describe a steady RANS simulation, the simulation discussed in the current paper is unsteady. Therefore, in this paper, the effect of temporal variation of  $\Delta\dot{Q}_i(t)$  can be analysed. The heat release rate  $\Delta\dot{Q}_i(t)$  is found by integration of the volumetric density of the local heat release rate  $\dot{q}$  over the volume  $\Delta V_i(t)$ , which is the part of the domain for which  $\tau(\vec{x}, t)$  is in the range  $\tau_i \pm \Delta\tau/2$

$$\Delta\dot{Q}_i(t) \equiv \int_{\Delta V_i(t)} \dot{q}(\vec{x}, t) dV \quad (2)$$

Since  $\tau(\vec{x}, t)$  is a function of time, so is  $\Delta V_i(t)$ . The index  $i$  correspond to discrete ranges of time delay  $\tau$ . Figures 5 and 6 give a visual impression of the variation of the variables  $\dot{q}$  and  $\tau$  in the flame region. The left hand side of equation (2) is normalised and presented as the histogram

$$H_i(t) \equiv \frac{\Delta\dot{Q}_i(t)}{\Delta\tau P_{\text{th}}} \quad (3)$$

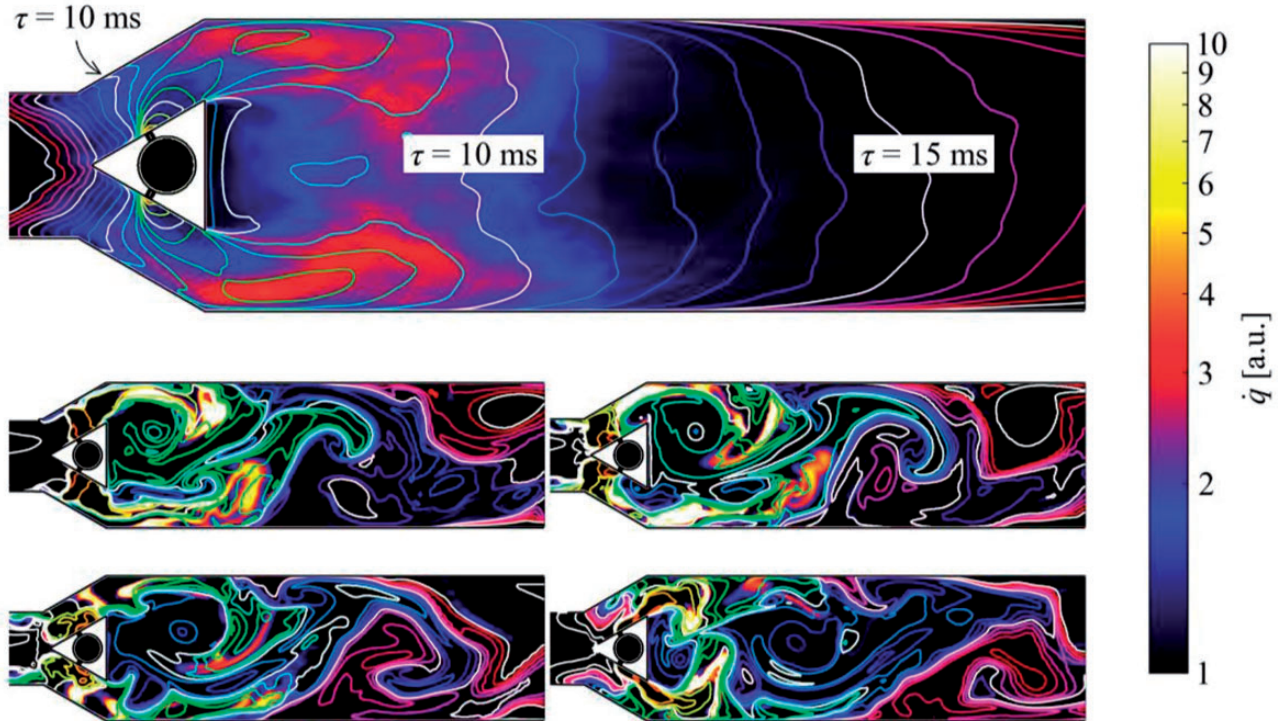


**Figure 5.**  $\tau$  as contour lines and  $\dot{q}$  as background colouring for Hummer: time-average on top gives a quantitatively more readable impression. Qualitatively, the instantaneous fields (for arbitrary time steps) shown below look very different.

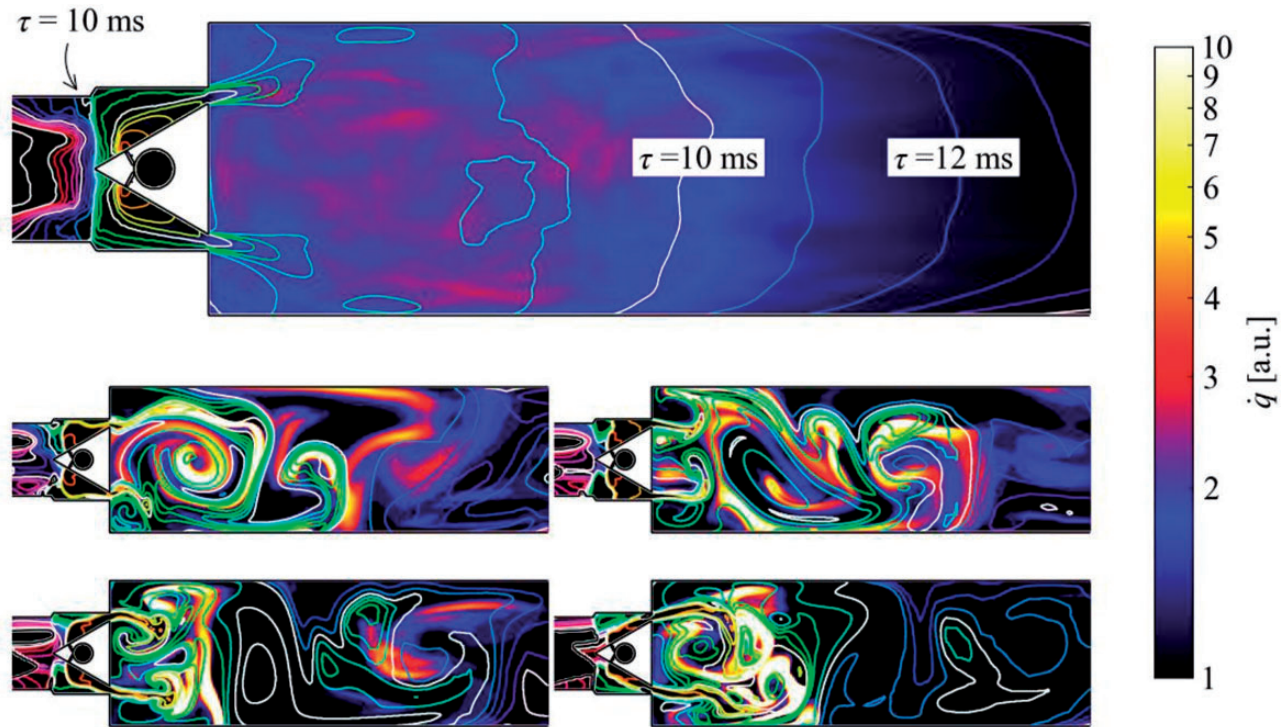


**Figure 6.**  $\tau$  as contour lines and  $\dot{q}$  as background colouring for Limousine: time-average on top gives a quantitatively more readable impression. Qualitatively, the instantaneous fields (for arbitrary time steps) shown below look very different.

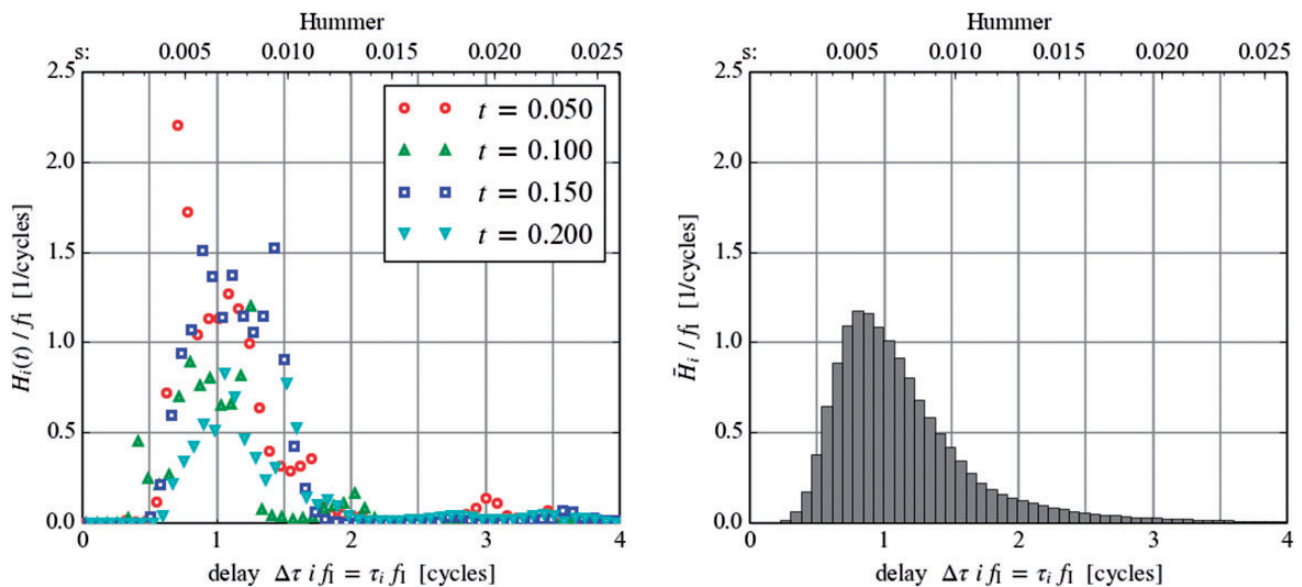


**Figure 7.** Momentary distributions  $H_i(t)$  on the left; most fuel is combusted roughly one period of oscillation (7 ms) after it was injected. Averaging over a large number of time steps leads to the much smoother histogram  $\bar{H}_i$  on the right.

where  $P_{th}$  is the nominal (constant) thermal power.  $H_i(t)$  is now the normalised momentary heat release rate, associated with combustion of fuel that was injected in the interval  $t - \tau_i \pm \Delta\tau/2$ , see Figure 7. The total momentary heat release rate is  $\dot{Q}(t) = P_{th} \sum_i H_i(t)\tau$ ,

i.e. the heat release at time  $t$ , associated with fuel injected at any time  $t - \tau$  in the past. As Figure 7 shows, there is strong temporal variation in overall heat release, mean  $\tau$ , and shape of the distribution. The time-averaged distribution  $\bar{H}_i$  is much smoother.

Since the amount of unburned fuel leaving the domain is negligible

$$\frac{\dot{Q}(t)}{\bar{Q}} \approx \frac{\dot{Q}(t)}{P_{\text{th}}} = \sum_i H_i(t) \Delta \tau \quad (4)$$

Consequently, the time-average  $\sum_i \bar{H}_i \tau$  will approach unity for long averaging time intervals.

The momentary heat release of a (lean) flame depends on the density  $\rho$ , local equivalence ratio  $\Phi$ , the flame surface  $A_{\text{fl}}$ , and the local burning velocity  $S_L$ , as

$$\dot{Q}(t) \propto \int_{A_{\text{fl}}(t)} \rho(\vec{x}, t) \Phi(\vec{x}, t) S_L(\vec{x}, t) dA \quad (5)$$

The local equivalence ratio  $\Phi(\vec{x}, t)$  along the flame front will first of all change in response to modulation of the fuel mass flow  $\dot{m}_F$ , resulting in corresponding changes in the overall heat release rate. It is assumed in the following, that this is the dominant mechanism by which the flame responds to controller action, i.e. this is the main mechanism by which control authority is realised. There will be additional contributions to the heat release rate, that result from fluctuations of  $S_L$  and  $A_{\text{fl}}$ :

For lean flames, burning velocity is proportional to equivalence ratio, so that  $S_L$  will fluctuate in phase with  $\Phi$ . This second contribution to the heat release rate will lead to a slight increase in the effect of active control, independent of controller settings and combustor geometry. This paper is primarily concerned with a comparison between two combustors. Since this second effect influences both combustors similarly, it does not affect the comparison and will be neglected in the following.

Finally, there will be a third contribution to the fluctuations in heat release rate due to changes in flame surface area  $A_{\text{fl}}$ . This is a secondary effect, which results from modulation of the local burning velocity, as shown by Huber and Polifke.<sup>21,22</sup> Due to the strong fluctuation of the shape of the current flame, influenced by large-scale vortical structures, the coherent response of  $A_{\text{fl}}$  is expected to be minimal and will be neglected in the following as well.

Taking the time delay into account, the change in momentary heat release due to a modulation of injected fuel mass flow  $\dot{m}_F$  is estimated as

$$\frac{\dot{Q}'_i(t)}{\bar{Q}} \approx \sum_i \frac{\dot{m}'_F(t - \tau_i)}{\bar{m}_F} H_i(t) \quad (6)$$

Conceptually,  $H_i(t)$  is now similar to, but different from an impulse response, insofar that  $H_i(t)$  relates the

heat release rate at the current time  $t$  to fuel injection over the past times  $t - \tau$ . A conventional impulse response would relate heat release at  $t + \tau$  in the future to fuel injection at current  $t$ . Besides,  $H_i(t)$  is a function of time, strongly influenced by turbulent vortical structures and temporal variation in flame shape, while an impulse response only describes response coherent to the input. These effects will average out over many time steps, so that in the following, the time-averaged distribution  $\bar{H}_i$  will be interpreted as an estimation of the impulse response relating heat release rate to fuel flow modulation. The discrete Fourier transform of  $H_i(t)$  with respect to  $i$  is  $T_j(t)$

$$\frac{\dot{Q}(f_j, t)}{\bar{Q}} \approx \frac{\dot{m}_F(f_j, t)}{\bar{m}_F} T_j(t) \quad (7)$$

Note that like  $H_i(t)$ ,  $T_j(t)$  is a function of time. The time-averaged function  $\bar{T}_j$  is taken as an approximation of the transfer function relating heat release rate to fuel flow modulation. Dispersion of the delay  $\tau$  due to mixing will lead to a reduction of the magnitude of this transfer function as discussed by Mehta et al.<sup>23</sup> The influence of temporal fluctuation of  $T_j(t)$  will be discussed in the following section.

## Results

The simulation was run without control for a total time of 0.2 s. The oscillation develops quickly, as shown in Figure 8, and mode shapes are evaluated between 0.036 s and 0.2 s. After applying a Blackman window to the time domain data, the frequency of the dominant mode was estimated from the Fourier-spectrum. The mode shapes, i.e. amplitude and phase as a function of  $x$ , were acquired through evaluation of the Fourier coefficients corresponding to the estimated frequencies.

### Oscillation without control

The mode shapes found this way are presented in Figure 9. Phase is defined to be zero for the (spatial mean) pressure at the flame. Besides the difference in amplitude and frequency, the Limousine shows a deeper cusp in amplitude at the flame holder, and a significant jump in phase, both caused by the blockage due to the narrow slits around the flame holder.

### Controller settings and analysis of the convective time delay

The value of the convective time delay at the flame is interpreted in the form of the distribution  $H_i(\tau)$  of the heat release. This quantity is plotted for both

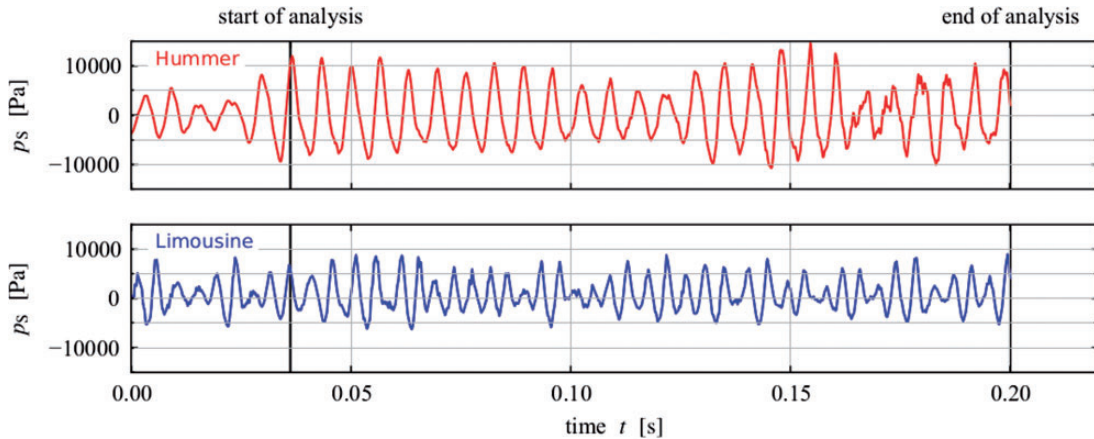


**Figure 8.** Time trace of the pressure at the 'sensor' for both combustors running without active control.

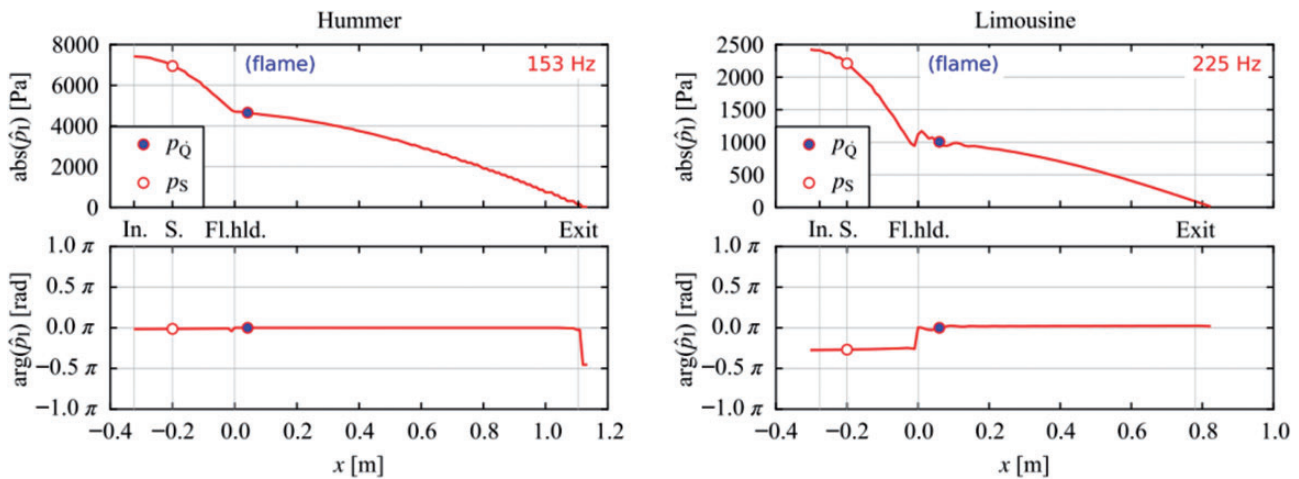


**Figure 9.** Mode shapes without active control; left: Hummer, right: Limousine.

combustors in the upper half of Figures 10 and 11. The peak of the heat release lies around  $\tau \approx 6$  ms for the Hummer and 8 ms for the Limousine which is similar to the values  $10 \pm 2$  ms found by Krebs and Lohrmann<sup>19</sup> on their swirl burner, so that in perspective of this parameter the laboratory combustors are representative of industrial combustors.  $T_j(t)$  is shown in the form of a colour wheel graph below. The amplitude  $\text{abs}(T)$  is expressed by the lightness of the colour, while the hue represents the argument  $\text{arg}(T)$ . The low-frequency limit of  $T$  approaches unity (bright red). For higher frequencies, the absolute value  $\text{abs}(T)$  decreases to zero, shown as black, while the argument  $\text{arg}(T)$  drops (from red to blue and green etc.) and shows more and more time-wise fluctuation. It can be estimated from the lower plot in Figure 10, that the phase shift between fuel injection and heat release is about  $0.3\pi = -1.7\pi$  (with quite some variation around this value), i.e. the fuel is consumed almost a full cycle

after it is injected into the air flow. This corresponds approximately to the peak of  $H$ , while the mean of  $H$  lies at a significantly higher value of  $\tau$ .

The Limousine rig has a longer delay time in seconds, as shown in Figure 11. This difference is even greater when expressed in cycles of the dominant frequency, since this combustor has a higher resonant frequency. Moreover, the flame is less compact in stream-wise direction, so the histogram  $H$  is much wider than for the Hummer. Looking at the colour wheel graph for the Limousine,  $\text{arg}(T)$  at the dominant frequency  $f_1$  varies so strongly over time that it is not possible to estimate the required controller phase shift from this graph.

To get a more accurate reading, the time-averaged value  $\bar{T}_j$  is presented in a Bode plot. The controller phase shift  $\Delta\varphi_{ATC}$  was set according to equation. (1), using  $\text{arg}(T)$  instead of the term  $(\tau_{ac} + \tau_{cv})2\pi f_1$ .

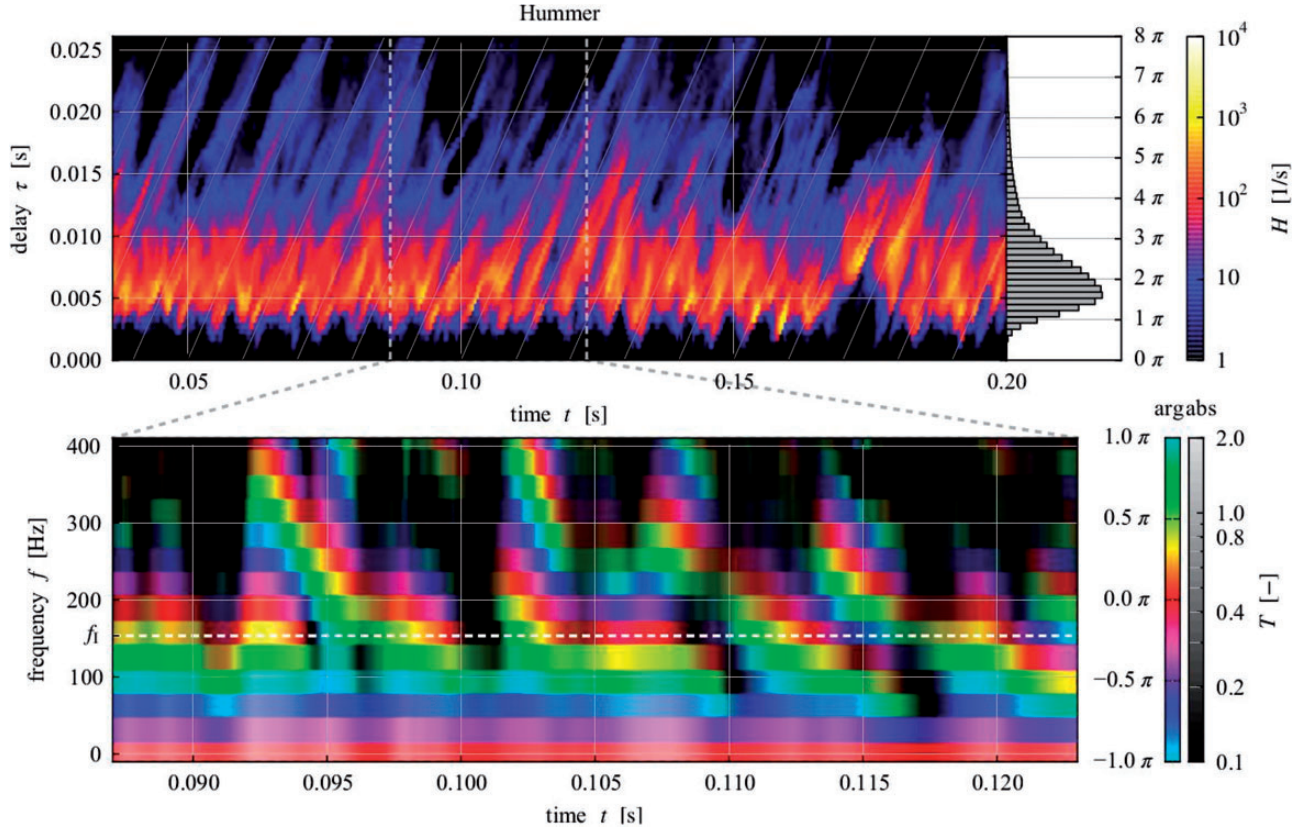


**Figure 10.** Above: Heat release in Hummer as a function of simulation time and time delay. The time-average distribution of the delay is shown as a histogram on the right. Below: Fourier-transforming the information above per time step gives an impression of the transfer function estimate  $T$  and its fluctuation over time.

The averaged transfer function  $\bar{T}_j = 1/(t_2 - t_1) \int_{t_1}^{t_2} T_j dt$ , averaged between  $t_1 = 0.036$  s and  $t_2 = 0.2$  s, is shown in Figure 12. The absolute value  $\text{abs}(\bar{T}_j)$  decreases with frequency due to two phenomena. First, a flame which is extended in the direction of the flow will lead to a flatter impulse response  $H_i(t)$  and a decrease in  $\text{abs}(T_j(t))$  for all  $t$ . Second, a variation of the time delay  $\tau$  over time leads to variation in phase  $\text{arg}(T_j(t))$  and after averaging to a lower absolute value  $\text{abs}(\bar{T}_j)$ . To give an impression of the relative importance of both effects, the root-mean-square of the absolute value,  $T_{j,\text{RMS}} = \sqrt{1/(t_2 - t_1) \int_{t_1}^{t_2} T_j T_j^* dt}$  is plotted as well.  $T_{j,\text{RMS}}$  decreases over frequency  $f_j$  due to  $\tau$ -wise dispersion alone, but is insensitive to variation of  $\text{arg}(T)$  over time. The distance between both lines is the standard deviation of the transfer function over time.

The absolute value  $\text{abs}(\bar{T})$  at the dominant frequency is an order of magnitude lower for the Limousine than for the Hummer. The value of  $T_{j,\text{RMS}}$  shows that this is not due to consistent, low value of  $\text{abs}(T_j(t))$  for all  $t$ , but much more due to the unsteadiness of  $H_i(t)$  of the Limousine rig.

Considering the high expected attenuation, the controller gain is set to the value of 0.03 %/Pa. This leads to a fuel flow modulation of  $\pm 100$  % for an amplitude of 3333 Pa. Not to influence the mean operating conditions, the controller signal is clipped between  $\pm 100$  %.

### Effect of active control

Both simulations were forked at  $t = 0.12$  s. The controller was activated with settings as described before. Figure 13 shows the time traces of pressure at the pressure probe. The pressure oscillation has clearly decreased for Hummer, but not for Limousine.

The corresponding spectra, plotted in Figure 14, can be compared more quantitatively. For Hummer, even the peaks at 300 and 550 Hz have been reduced significantly in amplitude, even though they lie outside of the frequency range in which the controller is active. The decrease in the peak at 300 Hz is expected, since this peak is a higher harmonic of the dominant oscillation. The peak at 550 Hz is the independent 3/4 wave mode. Recalling Figure 12, no control authority was expected for these higher frequencies either. The results for

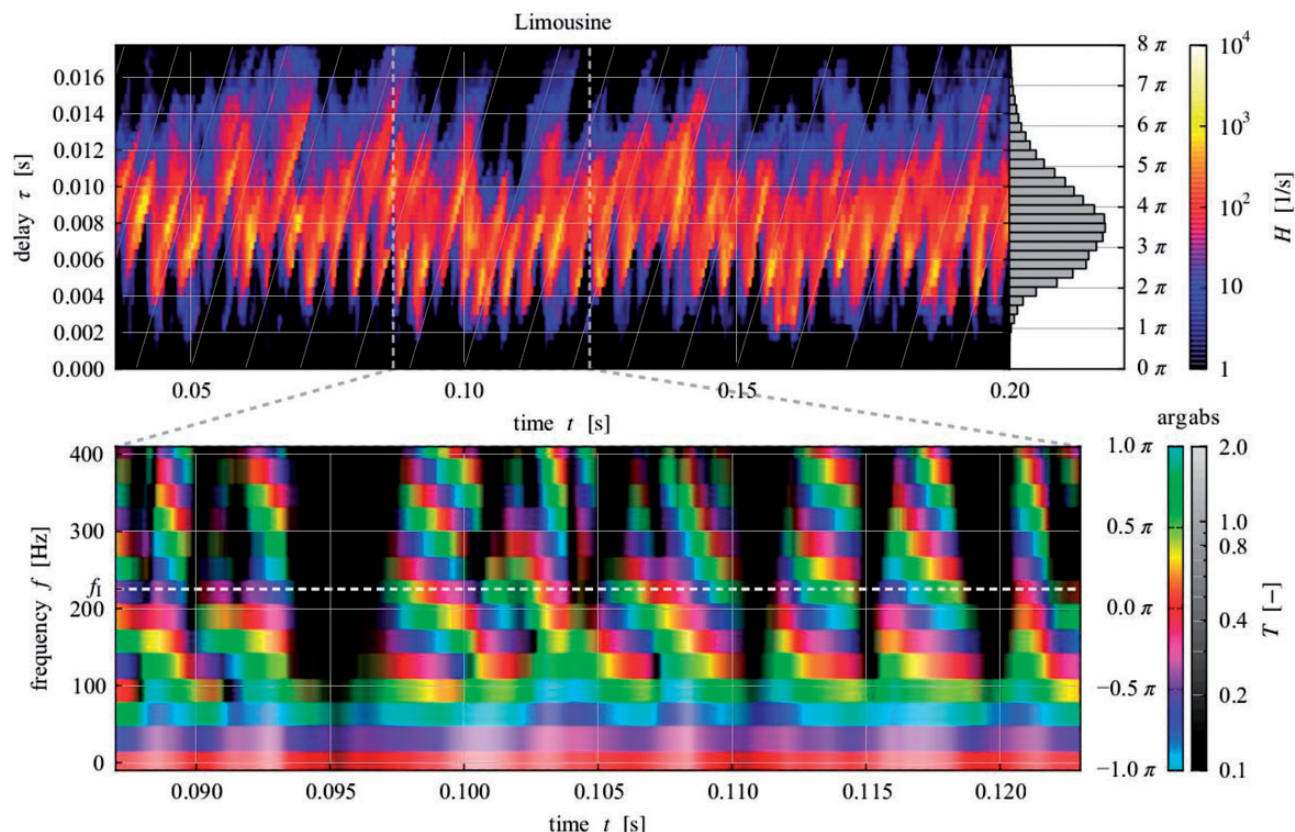


**Figure 11.** Above: Heat release in Limousine as a function of simulation time and time delay. The time-average distribution of the delay time is shown as a histogram on the right. Below: Transfer function estimate  $T$  acquired by Fourier transformation of the upper plot, and its fluctuation over time. The phase of the estimated transfer function at the dominant oscillation frequency shows much more variation than for the Hummer.

Limousine on the other hand show no structural increase or decrease of the pressure fluctuations.

The results shown in Figure 14 compare well to the experimental results given in Figure 1, at least in terms of amplitude and frequency of the dominant peaks. Minor peaks and general spectral distribution shows some discrepancy. The experimental results show smoother spectra, and a lower noise level, since the results could be averaged over a longer time to get statistically more meaningful results.

Now it is interesting to see whether the convective delay has changed due to the operation of active control. To this end, the same analysis as applied to the uncontrolled simulation in ‘Controller settings and analysis of the convective time delay’ was applied to the controlled case, leading to Figure 15.

For Hummer, the controlled flame extended further downstream. In this case, the changes lead to less control authority (decrease of  $\text{abs}(\bar{T}_j)$ ), and more interestingly, a shift in the phase of  $\bar{T}$ , which decreases the effect of control with the previously set phase shift. For the Limousine rig, the changes in flame shape are much less.

The limitations on active control, posed by time delay, are discussed by Cohen and Banaszuk.<sup>24</sup> The suppression of the oscillation on the Hummer combustor might be improved by adapting the phase shift to the change in flame shape (for instance using the controller discussed by Banaszuk<sup>25</sup>). Experiments on the Hummer combustor showed that the amplitude of the pressure fluctuation was not always a smooth function of the controller settings, nor was it always single-valued, so that both a stable and unstable state could be found for those conditions. This poses a serious threat to the robustness of adaptive control on this combustor.

## Discussion and conclusion

Two combustors were modelled in ANSYS CFX. Active control was implemented analogous to experiment by modulation of the fuel mass flow. The distribution of the convective time between fuel injector and flame is evaluated and used as an estimate for the impulse response relating fuel mass inflow and heat release. Controller settings were based on results from

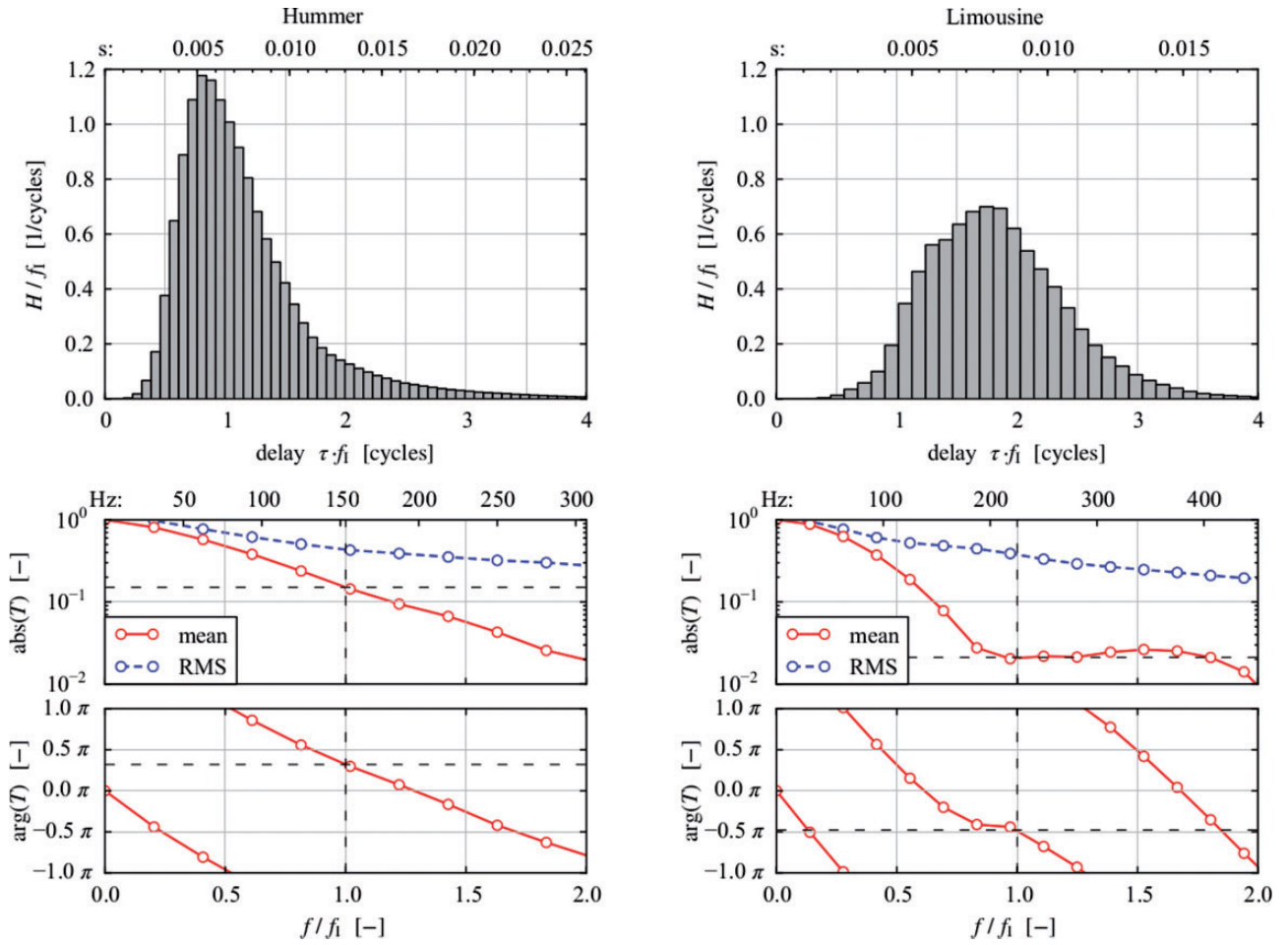


**Figure 12.** Expected impulse response (above) and transfer function (below) relating fuel injection fluctuation to heat release. For the absolute value, both the time-averaged  $\text{abs}(T_j)$  as well as the time-wise RMS,  $T_{j,\text{RMS}}$ , are shown. Left: Hummer, right: Limousine. Frequencies are non-dimensionalised with the respective dominant oscillation frequency.

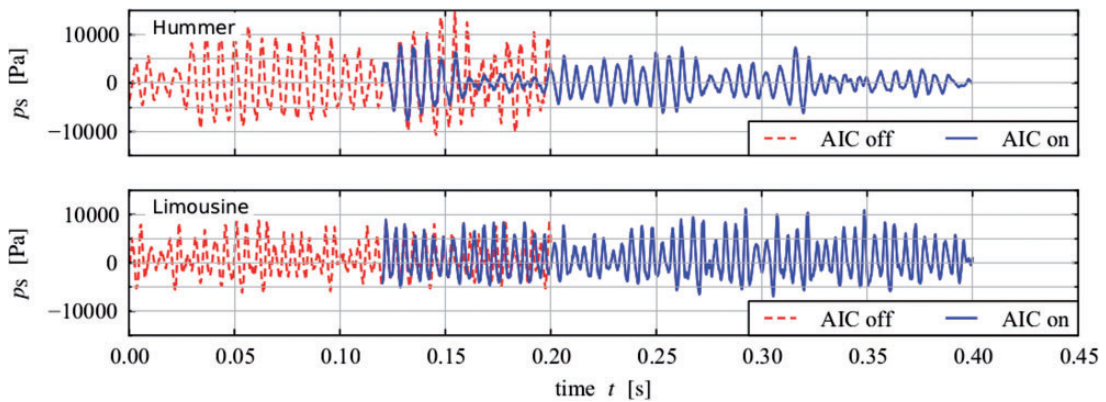


**Figure 13.** Time trace of pressure at sensor without and with control for both combustors.

a simulation without active control. The effectiveness of active control was demonstrated on the Hummer rig. Active control was unsuccessful on the combustor the Limousine rig in experiment, for reasons then not

properly understood. The computational results suggest that the dispersion and temporal variation of the convective time delay are decisive for success or failure of active control by fluctuation of the fuel mass flow.

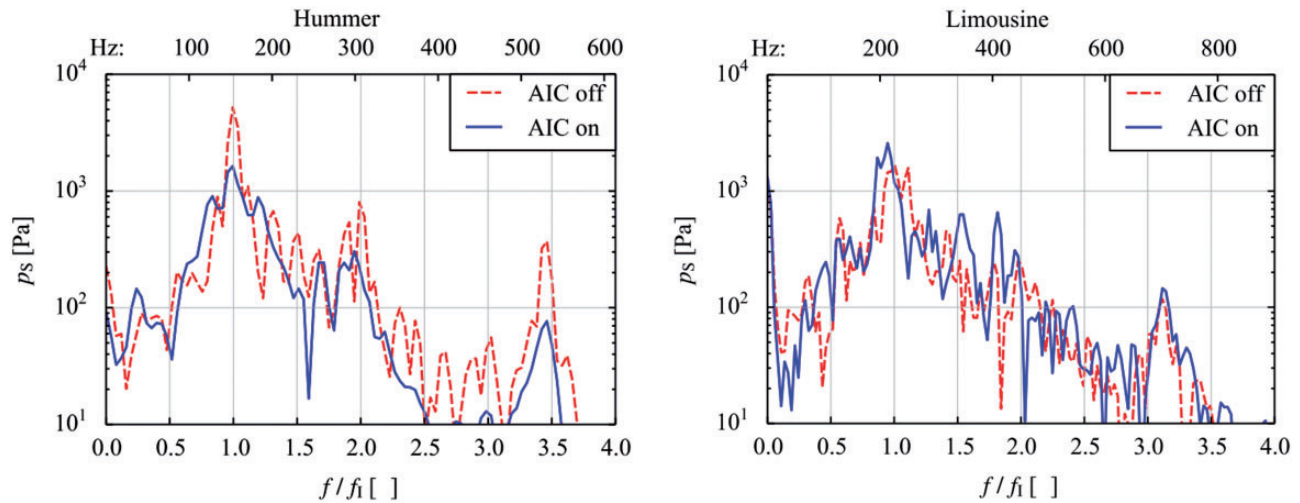


**Figure 14.** Comparison of spectra with and without active control. The frequencies are normalised using the uncontrolled peak frequency.

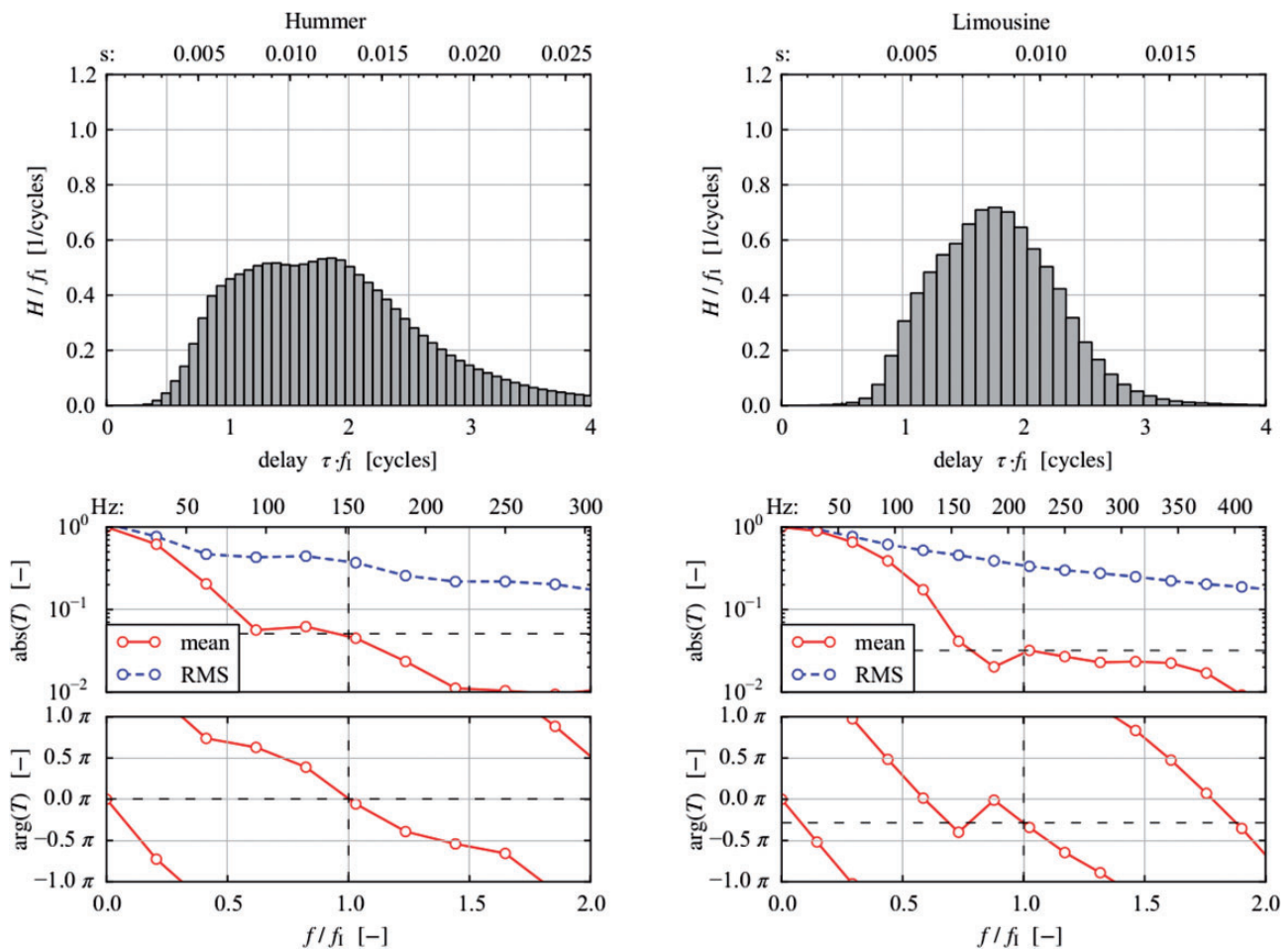


**Figure 15.** Metrics analogous to Figure 8 with active control applied. Left: Hummer, right: Limousine. While Limousine shows little change compared to the previous situation, active control led to a longer flame further downstream for Hummer.

These criteria can be used for engineering applications. Generally, this form of actuation for active control is considered problematic when either the dispersion or temporal variation of  $\tau$  is too large, e.g. when the flame is too long, or stabilised too far downstream of the fuel injector, or when mixing causes too much dispersion in the convective time between the injector and the flame. When a combustor has only one fuel injector, a conflict of interest can exist. For stable operation a wide dispersion in time delay is preferable,<sup>20</sup> while a narrow dispersion is preferable for active control. In any case, a reliable, constant time delay makes a combustor more reliable in operation. If a combustor has multiple fuel injectors, it is advisable to apply active control on those injectors closest to the flame, as was done by Hermann and Orthmann.<sup>8</sup>

In ‘Definition of the convective time’ section, the response of the heat release to fluctuations of the fuel mass flow was estimated, disregarding the influences of flame surface  $A_{fl}$  and the flame speed  $S_L$ . The impulse response is estimated as the distribution of the heat release  $\dot{Q}$  over convective time  $\tau$ .

In the case of the Hummer combustor, the average flame shape changed significantly due to the action of active control. So that ideally the controller settings could be updated. The initial settings for the Hummer combustor were effective enough to realise a significant reduction in pressure amplitude, legitimating the assumptions made in ‘Definition of the convective time’ section for this case.

In the case of the Limousine burner, the flame shape varies much more strongly and chaotically over time. It is therefore assumed that the coherent influence of  $A_{fl}$  and  $S_L$  on the impulse response are negligible. Follow-up research might give a more definitive answer. System identification could be performed by analysis of the reaction of the flame to uncorrelated fluctuation of the flame, but this would take a much longer simulated time before the controller could be started.

### Acknowledgements

ANSYS Inc. was a project partner in LIMOUSINE and supported this work with licenses. Phil Stopford deserves special thanks for his invaluable advice on the use of CFX. This publication owes greatly to his support. Finally, we would like to thank Robert Widhopf-Fenk for making the controller algorithm available in a form that could be connected to CFX, and Constanze Temmler, whose preliminary work helped setting up the computations presented in this paper.

### Declaration of conflicting interests

The author(s) declared no potential conflicts of interest with respect to the research, authorship, and/or publication of this article.

### Funding

The author(s) disclosed receipt of the following financial support for the research, authorship, and/or publication of this article: This work was done in context of the EU-funded Marie Curie research project LIMOUSINE (FP7-214905). The financial support from the European commission is gratefully acknowledged.

### References

1. Culick FEC. *Unsteady motions in combustion chambers for propulsion systems*. Technical Report. Report no. RTO-AG-AVT-039, RTO/NATO, 2006, <https://www.cso.nato.int/pubs/rdp.asp?RDP=RTO-AG-AVT-039>.
2. Lang W, Poinot T and Candel S. Active control of combustion instability. *Combust Flame* 1987; 70: 281–289.
3. Bloxside GJ, Dowling AP, Hooper N, et al. Active control of reheat buzz. *AIAA J* 1988; 26: 783–790.
4. Heckl MA. Active control of the noise from a Rijke tube. *J Sound Vib* 1988; 124: 117–133.
5. Hermann J, Gleis S and Vortmeyer D. Active instability control (AIC) of spray combustors by modulation of the liquid fuel flow rate. *Combust Sci Tech* 1996; 118: 1–25.
6. Dowling AP and Morgans AS. Feedback control of combustion oscillations. *Annu Rev Fluid Mech* 2005; 37: 151–182.
7. Culick FEC and Palm S. Active control of combustion after twelve years efforts. *Prog Propul Phys* 2009; 1: 441–468.
8. Hermann J and Orthmann A. Combustion dynamics: application of active instability control on heavy duty gas turbines. In: *Paper presented at the RTO AVT Course on “Active Control of Engine Dynamics”*, Brussels, Belgium, 14–18 May 2001, <https://www.cso.nato.int/pubs/RDP.asp?RDP=RTO-EN-020>.
9. Kosztin B, Heckl M, Müller RAJ, et al. Instabilities in a model gas turbine combustor: theory and experiment. In: *17th International Congress of Sound and Vibration (ICSV17)*, Cairo, Egypt, 2010.
10. Menon S. Active Combustion control in a ramjet using large-eddy simulations. *Combust Sci Tech* 1992; 84: 51–79.
11. Menon S. Secondary fuel injection control of combustion instability in a ramjet. *Combust Sci Tech* 1995; 100: 385–393.
12. Shinjo J, Matsuyama S, Mizobuchi Y, et al. Study on flame dynamics with secondary fuel injection control by large eddy simulation. *Combust Flame* 2007; 150: 277–291.
13. Menter FR and Egorov Y. The scale-adaptive simulation method for unsteady turbulent flow predictions, part 1: theory and model description. *Flow Turbul Combust* 2010; 85: 113–138.
14. Müller CM, Breitbach H and Peters N. Partially premixed turbulent flame propagation in jet flames. *Symp (Int) Combust* 1994; 25: 1099–1106.
15. Polifke W, Flohr P and Brandt M. Modeling of inhomogeneously premixed combustion with an extended TFC model. *J Eng Gas Turbines Power* 2002; 124: 58–65.

16. Zimont VA, Polifke W, Bettelini M, et al. An efficient computational model for premixed turbulent combustion at high Reynolds numbers based on a turbulent flame speed closure. *J Eng Gas Turbines Power* 1998; 120: 526–532.
17. Forkel H. Modification to the burning velocity model at ANSYS Germany. Private communication, 2012.
18. Putnam AA and Dennis WR. Burner oscillations of the gauze-tone type. *J Acoust Soc Am* 1954; 5: 716–725.
19. Krebs W and Lohrmann M. Thermoacoustic flame response of swirl flames. *Proc ASME Turbo Expo* 2002; 333–344. DOI: 10.1115/GT2002-30065.
20. Polifke W, Kopitz J and Serbanovic A. Impact of the fuel time lag distribution in elliptical premix nozzles on combustion stability. In: *7th AIAA/CEAS Aeroacoustics Conference*, AIAA 2001-2104, Maastricht, Netherlands, 28–30 May 2001.
21. Huber A and Polifke W. Dynamics of practical premixed flames, part I: model structure and identification. *Int J Spray Combust* 2009; 1: 199–228.
22. Huber A and Polifke W. Dynamics of practical premixed flames, part II: identification and interpretation of CFD data. *Int J Spray Combust* 2009; 1: 229–249.
23. Mehta P, Banaszuk A and Soteriou M. Impact of convection and diffusion processes in fundamental limitations of combustion control. In *2nd AIAA Flow Control Conference*. American Institute of Aeronautics and Astronautics, Portland, Oregon, 28 June–1 July 2004.
24. Cohen JM and Banaszuk A. Factors affecting the control of unstable combustors. *J Propul Power* 2003; 19: 811–821.
25. Banaszuk A, Ariyur KB, Krstić M, et al. An adaptive algorithm for control of combustion instability. *Automatica* 2004; 40: 1965–1972.